

A Tight-Binding Approach to Creating van der Waals Metamaterials

Syeda Minhal Gardezi

Submitted in Partial Fulfillment of the
Prerequisite for Honors in Physics

Wellesley College
Harvard School of Engineering and Applied Sciences

May 2020

© Syeda Minhal Gardezi

Acknowledgements

I would first like to thank the metamaterials group of the Hoffman Lab at Harvard University. This thesis would not have been possible without the endless support and countless opportunities Professor Jenny Hoffman has given me during what can only be described as the most chaotic year of my life. I also owe many thanks to Harry Pirie for finding so much time in his legendarily busy schedule to mentor a frightened Wellesley student. Thanks as well to Nathan Drucker for his invaluable guidance and support and to Will Dorrell and Ben November for being such welcoming collaborators. Finally, I'd like to thank Fan Du and Radu Andrei for their help and friendship throughout my time at Harvard, and Jennifer Wang for being my inside man.

I of course owe endless thanks to my thesis advisor, Professor Robbie Berg. He has been a mentor to me since my first semester at Wellesley and he is responsible for every major opportunity I've received while here. Thank you for offering me a position in your diamond lab two summers ago, and for introducing me to and including me in the Center for Integrated Quantum Materials. Thank you for encouraging my creativity alongside my academic skills, from praising my iPad notes and drawings in class to believing in my fully-realized binary clock in PHYS 310. Thank you for putting up with my sporadic communication this year and for being so understanding throughout this global crisis.

Thank you as well to the rest of the Physics department, especially Professor Katie Hall, who offered me reassurance and inspiration at my lowest points, Professor Yue Hu, who constantly looked out for and encouraged me, and Professor Becky Belisle for agreeing to join my thesis committee after our first extended conversation together. The Physics professors of Wellesley have truly led me through these past four years and I consider them lifelong mentors and friends.

Thank you to the rest of the Physics majors at Wellesley for being such empathetic and silly geniuses.

Thank you to my wonderful friends at Wellesley and at home, none of whom study Physics or understand what I am talking about at any given moment. I could not have made it this far without you.

And, of course, thank you to my brothers for inspiring me to reach for big things, and to my mother, for giving me everything I have.

Abstract

Van der Waals heterostructures are a fertile frontier for discovering emergent phenomena in condensed matter systems. They are constructed by stacking elements of a large library of two-dimensional materials, which couple together through van der Waals interactions. However, the number of possible combinations within this library is staggering, and fully exploring their potential is a daunting task. Van der Waals metamaterials are designed to reshape the flow of acoustic waves to mimic electron motion. It has been previously shown that the van der Waals interaction can be mimicked in metamaterials through the use of an interlayer coupling membrane. I now present a method for designing new van der Waals metamaterials following tight-binding principles. I first present the connected-cavity model for designing two-dimensional metamaterials. I then demonstrate the effectiveness of the model by creating metamaterial graphene, AA- and AB-stacked metamaterial bilayer graphene, and metamaterial twisted bilayer graphene.

List of Figures

1.1	(a) A one-dimensional Bravais lattice has periodicity a . (b) A two-dimensional rectangular Bravais lattice has primitive lattice vectors \vec{a}_1 and \vec{a}_2 .	1
1.2	There is no unique choice of primitive vectors for a Bravais lattice. Here we see just four possible sets of primitive vectors for the triangular lattice, but there are in fact an infinite number of possibilities.	2
1.3	(a) Each point in the triangular lattice is equivalent to every other point, making it a Bravais lattice. (b) In the honeycomb lattice, points A and B are equivalent but A and C are not, meaning it is not a Bravais lattice.	3
1.4	The honeycomb lattice has many possible unit cells (red) and primitive cells (green). While generic unit cells may contain any number of lattice points, each primitive cell contains only one lattice point. Widely-used conventional unit cells (blue) contain two lattice points.	4
1.5	A two-dimensional hexagonal Brillouin zone has high-symmetry k points Γ (green, at the center of the Brillouin zone), K (blue, at the vertices of the hexagon, with adjacent K points differentiated as K and K'), and M (red, at the midpoint of the hexagon edges).	5
1.6	The energy needed for an electron to hop to a nearest neighbor if t . Each gray bar connects nearest neighbors. One pair of nearest neighbors is shown in red; one pair of next-nearest neighbors is shown in green; one pair of next-next-nearest neighbors is shown in blue.	6
2.1	Two honeycomb lattices twisted relative to each another form periodic Moiré patterns at certain commensurate angles. The conventional unit cell of the overall Moiré pattern (red) increases in size as the twist angle (θ) decreases. When $\theta = 0^\circ$, the system is bilayer graphene and its unit cell is the same size as graphene's. When $\theta = 21.8^\circ$, the twisted bilayer supercell contains 7 graphene unit cells; when $\theta = 9.43^\circ$, the supercell contains 37 graphene unit cells; when $\theta = 5.09^\circ$, the supercell contains 127 graphene unit cells.	9

3.1	Here we visualize a 2SB honeycomb lattice of connected cavities as the basic design for phononic metamaterial graphene. Channels connect nearest neighbor hopping sites. Nearest neighbor hopping (t) occurs either from an A_1 site to an A_2 site or vice versa.	15
3.2	(a) This unit cell for 2SB metamaterial graphene shows air cavities in purple, steel in opaque gray, and HDPE bounding layers in semi-transparent gray. Here $a = 10$ mm, $R = 3.5$ mm, $w = R/4 = 0.875$ mm, and $D = 1$ mm. (b) The metamaterial's resulting band structure displays an isolated Dirac-like crossing (blue) mimicking graphene.	16
3.3	Unconnected-cavity sites (A_3) have been added to the original honeycomb lattice of connected cavities. Channels connect nearest neighbor hopping sites (with hopping energy t); there is no hopping from A_1 or A_2 sites to A_3 sites.	16
3.4	(a) The unit cell for 3SB connected-cavity metamaterial graphene has the same properties as the unit cell in Figure 3.2(a). The additional unconnected cavities have radius $r = 0.75R = 2.625$ mm. (b) The metamaterial's resulting band structure displays an isolated Dirac-like crossing (blue) identical to the one shown in Figure 3.2(b). The extra band (gray) represents an isolated air mode within the extra cavities.	19
3.5	Here we visualize the coupling between 2SB honeycomb cavity networks in either layer of AB-stacked metamaterial bilayer graphene. Connective channels within each layer indicate intralayer hopping (t); Overlapping sites have interlayer hopping (Δ). A_2 and B_1 sites overlap; A_1 and B_2 do not.	19
3.6	(a) This unit cell for 2SB AB-stacked metamaterial bilayer graphene shows air cavities in purple and steel in opaque gray. The metamaterial layers and outer HDPE bounding layers have the same properties (a , R , w , and D) as in Figure 3.2(a). The center coupling layer is HDPE with thickness D , identical to the outer bounding layers. (b) The metamaterial's resulting band structure displays abnormal behavior at the K point not matching the expected parabolic “kissing” structure present in AB-stacked bilayer graphene.	20
3.7	Here we visualize the coupling between 3SB honeycomb cavity networks in either layer of AB-stacked metamaterial bilayer graphene. Connective channels within each layer indicate intralayer hopping (t); Overlapping sites have interlayer hopping (Δ). A_2 and B_1 sites overlap as usual. A_1 sites overlap with B_3 sites and B_2 with A_3	21

3.8 (a) This unit cell for 3SB AB-stacked metamaterial bilayer graphene has the same properties as in Figure 3.6(a), with additional unconnected air cavities ($r = 2.626$ mm). (b) The metamaterial's resulting band structure displays parabolic “kissing” at the K point mimicking AB-stacked bilayer graphene. The extra two bands (gray) represent isolated air modes in A_3 and B_3 sites, respectively.	22
3.9 Here we visualize the coupling between 2SB honeycomb cavity networks in either layer of AA-stacked metamaterial bilayer graphene. Connective channels within each layer indicate intralayer hopping (t); Overlapping sites have interlayer hopping (Δ). Each cavity network overlaps entirely with the other; that is, A_1 sites overlap with B_1 sites and A_2 with B_2 . . .	23
3.10 (a) This unit cell for 2SB AA-stacked metamaterial bilayer graphene has the same properties as in Figure 3.6(a), with one metamaterial layer rotated 60° so that both cavity networks entirely overlap. (b) The metamaterial's resulting band structure displays double-Dirac-like crossings at the K point mimicking AA-stacked bilayer graphene.	24
3.11 Here we visualize the coupling between the 3SB honeycomb cavity networks in either layer of AA-stacked metamaterial bilayer graphene. Connective channels within each layer indicate intralayer hopping (t); Overlapping sites have interlayer hopping (Δ). There is overlap between A_1 and B_1 , A_2 and B_2 , and A_3 and B_3 sites.	25
3.12 (a) This unit cell for 3SB AA-stacked metamaterial bilayer graphene has the same properties as in Figure 3.8(a), with one metamaterial layer rotated 60° so that both cavity networks entirely overlap. (b) The metamaterial's resulting band structure retains the expected double-Dirac-like crossings at the K point seen in Figure 3.10(b). The extra two bands (gray) represent isolated air modes in A_3 and B_3 sites, respectively.	26
3.13 TBG has regions of AB stacking (blue triangles) and AA stacking (red circles) connected by transition regions that have neither AA nor AB stacking.	27
3.14 The Dirac-like crossings (blue) originally present in 3SB AA-stacked metamaterial bilayer graphene become flatter as θ decreases. Each band structure spans a smaller frequency range than the previous. Extra bands (gray) represent various other modes in the TBG heterostructure and are not relevant to the flattening bands.	27

3.15 (a) The metamaterial TBG supercells grow in size as θ decreases. Each supercell is composed of two 3SB metamaterial graphene layers (Figure 3.4) with an intervening HDPE coupling membrane, all sandwiched between two outer HDPE bounding membranes. As in all previously shown models, $a = 10$ mm, $R = 3.5$ mm, $r = 2.625$ mm, $w = 0.875$ mm, and $D = 1$ mm. (b) The band structures from Figure 3.14 are shown here plotted on the same frequency scale to visualize the flattening effect. Data is unavailable for the gray regions in the latter three band structures, but would contain additional extra bands (gray) irrelevant to the flattening Dirac-like crossings (blue).

28

Contents

Acknowledgements	i
Abstract	ii
List of Figures	iii
1 Introduction	1
1.1 Crystal Structure	1
1.2 Reciprocal Space	2
1.3 Tight-Binding	5
2 Motivating Metamaterials	8
2.1 Two-dimensional Materials and van der Waals Heterostructures	8
2.2 Metamaterials	10
2.3 Phononic Metamaterials as Quantum Mimics	10
2.4 Work Presented	11
3 Design Approach and Results	13
3.1 The Connected Cavity Model	13
3.2 Designing Two-dimensional Metamaterials	14
3.2.1 Graphene	15
3.3 Designing Stacked van der Waals Metamaterials	17
3.3.1 AB-Stacked Bilayer Graphene	17
3.3.2 AA-Stacked Bilayer Graphene	18
3.4 Designing Twisted van der Waals Metamaterials	21
3.4.1 Twisted Bilayer Graphene	22
4 Conclusion and Future Works	29
4.1 Expanding the Library of Two-dimensional Metamaterials	29
4.2 Magic-Angle Metamaterial Twisted Bilayer Graphene	29
4.3 Flat Band Metamaterials	30

Chapter 1

Introduction

1.1 Crystal Structure

Though the word “crystal” may call to mind angled gemstones, a true crystal is defined as a solid whose atoms are arranged in an ordered, periodic structure. As such, most solids, including metals, are crystalline in nature. The ideal crystal is structured as a **Bravais lattice**, an infinitely repeated pattern of identical units.

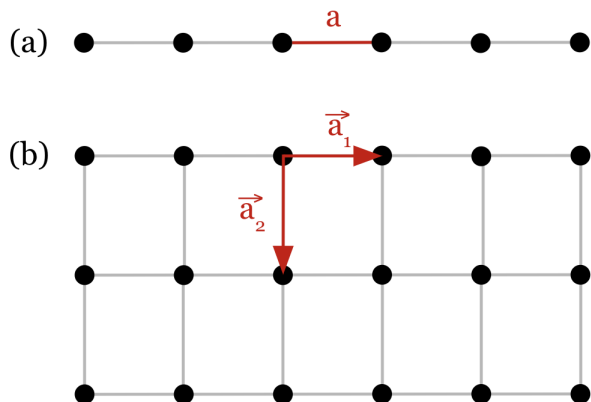


Figure 1.1: (a) A one-dimensional Bravais lattice has periodicity a . (b) A two-dimensional rectangular Bravais lattice has primitive lattice vectors \vec{a}_1 and \vec{a}_2 .

Let us consider the simplest Bravais lattice: a one-dimensional chain of points (Figure 1.1(a)). If we define the chain’s periodicity as a , the position of any point r is

$$r_n = na \quad n \in \mathbb{Z}.$$

Extending the lattice into two dimensions, let us consider a rectangular lattice of points (Figure 1.1(b)). We define this lattice’s periodicity through **primitive lattice vectors** \vec{a}_1 and \vec{a}_2 . The position of any point \vec{r} is then:

$$\vec{r}_{[n_1, n_2]} = n_1 \vec{a}_1 + n_2 \vec{a}_2 \quad n_1, n_2 \in \mathbb{Z}.$$

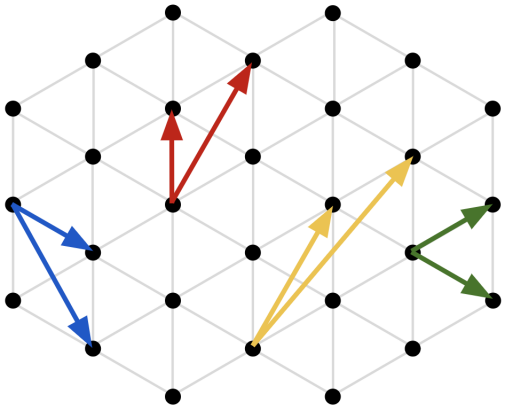


Figure 1.2: There is no unique choice of primitive vectors for a Bravais lattice. Here we see just four possible sets of primitive vectors for the triangular lattice, but there are in fact an infinite number of possibilities.

According to this definition, the choice of primitive lattice vectors is not unique (Figure 1.2)¹.

From these Bravais lattice definitions we see each lattice point has the same environment. In other words, the arrangement and orientation of the surrounding lattice appears exactly the same from the perspective of any point in a Bravais lattice.

In a non-Bravais lattice, however, each point is not necessarily equivalent to every other point. Consider the honeycomb lattice, which is similar to the triangular Bravais lattice but is not itself a Bravais lattice (Figure 1.3). To establish the periodicity of a non-Bravais lattice², we define a **unit cell**. A lattice unit cell is any region of a lattice that, when tiled out in space, reproduces the full lattice. A lattice's **primitive unit cell** is its smallest possible unit cell, containing only one point. However, for convenience, we often use a **conventional unit cell**, usually chosen to be as small as possible while maintaining the lattice's overall symmetries. There is no unique choice for any type of unit cell (Figure 1.4).

1.2 Reciprocal Space

While crystal structure is best described in real space, waves propagating through crystals are best described in reciprocal space³. The relationship between real space and reciprocal space is entirely analogous to the relationship between the time domain and frequency domain; we can switch between real and reciprocal space via Fourier transform.

If points in a real space lattice represent positions, a lattice in reciprocal space will

¹I have left out the explicit definitions for three-dimensional lattices because my research involves only two-dimensional materials. However, the mathematical definition for two-dimensional lattices can easily be extended to three dimensions by adding a third primitive lattice vector term. Again, the choice for all three vectors in that case would not be unique

²I will henceforth specify all Bravais lattices as such; the term “lattice” alone can refer to non-Bravais lattices like the honeycomb lattice.

³Reciprocal space is often called “momentum space” or “ k -space”.

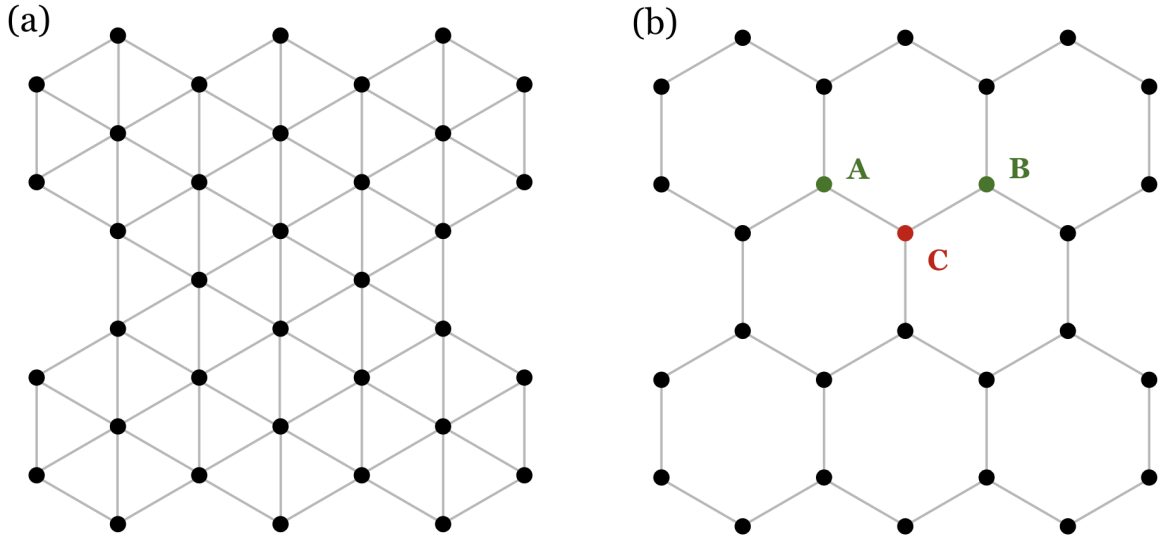


Figure 1.3: (a) Each point in the triangular lattice is equivalent to every other point, making it a Bravais lattice. (b) In the honeycomb lattice, points A and B are equivalent but A and C are not, meaning it is not a Bravais lattice.

have points representing wavevectors. Such a lattice is called the **reciprocal lattice**, and we can generate it by taking the Fourier transform of a real space lattice⁴.

Let us consider a lattice of points in real space defined \vec{R} . Consider also a generic plane wave e^{ikt} . The periodicity of plane wave will match the periodicity of the lattice only at certain values of \vec{k} . The set of such \vec{k} values in reciprocal space form the reciprocal lattice, which we will define as \vec{K} ⁵. From this definition we can say \vec{K} is the reciprocal lattice of \vec{R} if and only if

$$e^{i\vec{K}\cdot\vec{R}} = 1$$

for all points in the direct lattice.

The relationship between the periodicity of the direct and reciprocal lattices is outlined by the formula

$$\vec{b}_i \cdot \vec{a}_j = 2\pi\delta_{ij},$$

where δ_{ij} is the Kronecker delta⁶.

For a one-dimensional lattice R with periodicity a , the reciprocal lattice periodicity is simply $b = 2\pi/a$. That is, given $R_n = na$, $K_m = mb$, where m is an integer.

Similarly, a two-dimensional lattice \vec{R} with primitive lattice vectors \vec{a}_1 and \vec{a}_2 has a

⁴When described in respect to a reciprocal lattice, the real space lattice is known as the “direct lattice”.

⁵I am following Ashcroft & Mermin’s notation here [1], but other solid-state textbooks (like Simon’s [2]) may refer to the reciprocal lattice as \vec{G} .

⁶ $\delta_{ij} = 1$ for $i = j$ and is zero otherwise

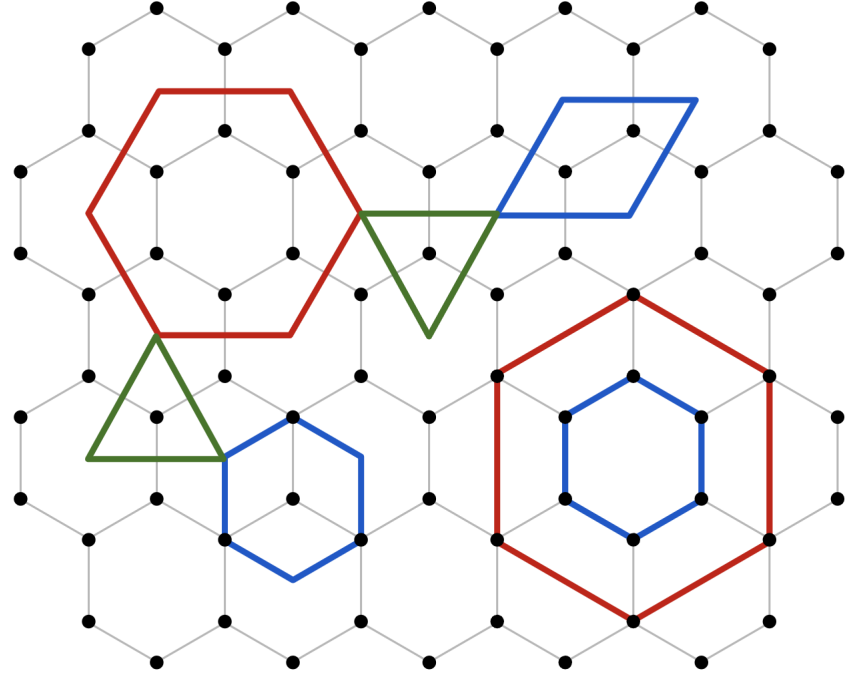


Figure 1.4: The honeycomb lattice has many possible unit cells (red) and primitive cells (green). While generic unit cells may contain any number of lattice points, each primitive cell contains only one lattice point. Widely-used conventional unit cells (blue) contain two lattice points.

reciprocal lattice with reciprocal primitive vectors

$$\vec{b}_1 = 2\pi \frac{\vec{a}_2 \times \hat{z}}{\hat{z} \cdot (\vec{a}_1 \times \vec{a}_2)} \text{ and}$$

$$\vec{b}_2 = 2\pi \frac{\hat{z} \times \vec{a}_1}{\hat{z} \cdot (\vec{a}_1 \times \vec{a}_2)}.$$

Or, for $\vec{R}_n = n_1 \vec{a}_1 + n_2 \vec{a}_2$, $\vec{K}_m = m_1 \vec{b}_1 + m_2 \vec{b}_2$ ⁷.

The primitive unit cell of the reciprocal lattice is known as the **Brillouin zone**. It contains all unique k points representing the periodicity of waves allowed in the original structure. Certain **high-symmetry points** exist in a Brillouin zone depending on the lattice's geometry⁸ (Figure 1.5).

Recalling the plane wave traveling through the direct lattice, the relationship between its frequency and wavevector is known as a **dispersion relation**. We can therefore plot the full dispersion of the wave by plotting its frequency at all points in the Brillouin zone. We only need to span the Brillouin zone because it is periodic. For example, if the

⁷Again, we can see how this formula may be applied to find the reciprocal primitive vectors in three dimensions, though I will not outline that here.

⁸ Γ always refers to the center of the Brillouin zone regardless of its geometry.

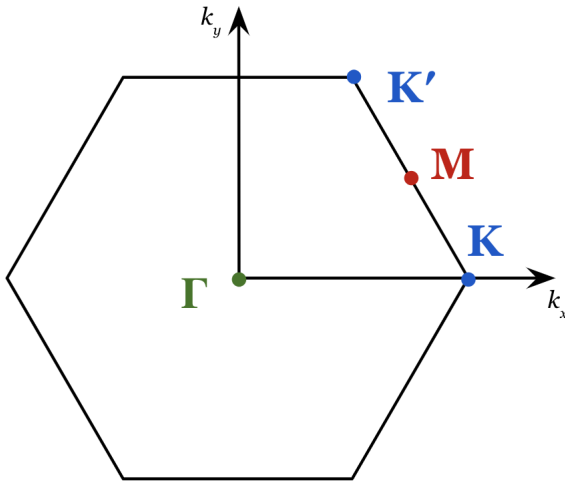


Figure 1.5: A two-dimensional hexagonal Brillouin zone has high-symmetry k points Γ (green, at the center of the Brillouin zone), K (blue, at the vertices of the hexagon, with adjacent K points differentiated as K and K'), and M (red, at the midpoint of the hexagon edges).

reciprocal lattice periodicity is $b = 2\pi/a$, the Brillouin zone centered around wavevector $k = 0^9$ will span $-\pi/a \leq k \leq \pi/a$, and $k \rightarrow k + 2\pi/a$.

The dispersion relation for an electron is analogously between its energy and momentum. The plotted dispersion for an electron is called a **band structure**.

1.3 Tight-Binding

To describe electron dynamics, we use the Hamiltonian operator $\hat{\mathcal{H}}$, which encodes the total energy of the system. When detailing the Hamiltonian for electrons in a crystalline solid, we may be tempted to incorporate each electron's interactions with every other electron; the resulting Hamiltonian would however be non-linear and almost certainly impossible to solve exactly. Instead, we consider the non-interacting Hamiltonian of a crystalline solid, simplified to the form

$$\hat{\mathcal{H}} = \hat{T} + \hat{V},$$

where \hat{T} is the kinetic energy operator and \hat{V} is the potential energy operator. \hat{V} arises from the ionic cores of atoms in the solid lattice and is therefore periodic in nature:

$$\hat{V} = V(\vec{r}) = \sum_n V_0(\vec{r} - \vec{r}_n)$$

There are two conventional techniques for solving this Hamiltonian to describe electron dynamics through a particular solid. First is the nearly-free electron model, which takes \hat{V} to be weak compared to \hat{T} . Qualitatively, under the nearly-free model, electrons are free to move throughout a solid with small perturbations due to the atomic lattice's periodic potential.

⁹This is known as the “first Brillouin zone”.

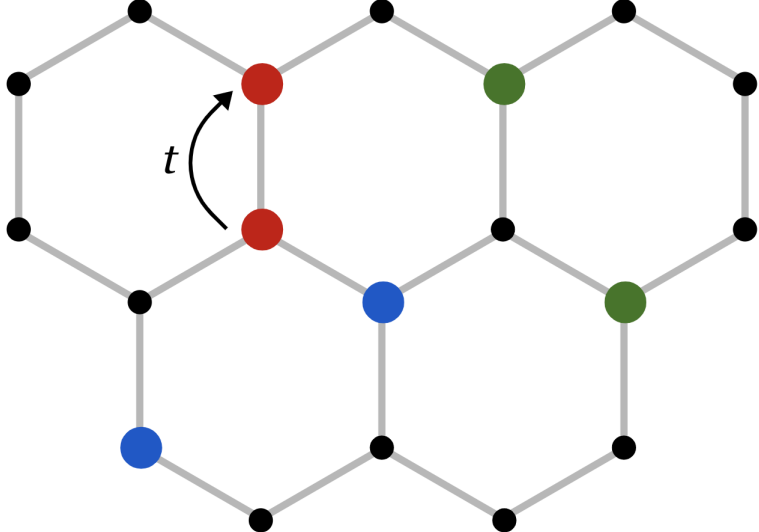


Figure 1.6: The energy needed for an electron to hop to a nearest neighbor is t . Each gray bar connects nearest neighbors. One pair of nearest neighbors is shown in red; one pair of next-nearest neighbors is shown in green; one pair of next-next-nearest neighbors is shown in blue.

The second technique, called the tight-binding model, takes the opposite limit of the nearly-free model, considering \hat{T} to be weak compared to \hat{V} . We then consider the single-electron bound states for each atom. With the approximation that the width of these bound states is small compared to the distance between lattice sites, the continuum model becomes a discrete one. That is, under the tight-binding model, electrons are bound to their atoms, rather than existing freely through the material.

The degree to which on-site wavefunctions between neighboring atoms in the lattice overlap determines electron coupling between sites. If two lattice sites are coupled, an electron has the opportunity to “hop” between sites. Electrons therefore travel through a material by hopping between neighboring lattice sites. From the perspective of one lattice site, the closest surrounding site the electron can hop to is called the “nearest neighbor”. Further sites are denoted “next-nearest neighbor”, “next-next nearest neighbor” and so on (Figure 1.6). We will assume there is a uniform distance between nearest neighbors¹⁰. The energy needed for an electron to hop to a nearest neighbor is t . If we let i and j denote nearest neighbor sites, we can write the tight-binding Hamiltonian as

$$\hat{\mathcal{H}}_{i,j} = t,$$

where the hopping rate between nearest neighbor sites is t^2 . It is more common, however, to examine the tight-binding Hamiltonian in its second quantized form:

$$\hat{\mathcal{H}} = t \sum_{i,j} (a_i^\dagger a_j + a_j^\dagger a_i)$$

where a_i^\dagger denotes the creation operator which projects an input state onto the site i and a_i is the annihilation operator, which removes an input state from i . In English, the tight-binding Hamiltonian shows the energy needed for an electron to be annihilated from a site j and then created at a site i , or vice versa.

¹⁰Graphically, a line connecting two lattice points denotes a pair of nearest neighbors (Figure 1.6).

Qualitatively, the tight-binding model allows us to intuitively consider electrons as particles hopping from site to site. Although this approximation may seem too simplistic to be accurate, the tight-binding model provides reasonably accurate solutions for the low-energy portions of electron spectra.

Chapter 2

Motivating Metamaterials

2.1 Two-dimensional Materials and van der Waals Heterostructures

Two-dimensional (2D) materials are crystalline structures comprised of very few atomic layers. This reduced dimensionality typically leads to enhanced quantum effects; 2D materials often display exceptional electronic, optical and magnetic properties [3, 4, 5, 6].

The first successfully isolated single-atom thick 2D material was graphene, formally discovered in 2004 [3]. Since then, the library of 2D materials has grown rapidly, providing a promising platform for studying emergent condensed matter phenomena.

2D materials can be stacked together, providing a wealth of novel quantum phenomena to explore. Individual 2D layers are held together by strong in-plane covalent bonds, while multiple layers in a stack are held together by weak out-of-plane van der Waals forces, making it easy to remove and replace 2D layers from a stack without damaging them [6]. Macroscopic stacks of 2D materials are appropriately called **van der Waals (vdW) heterostructures**.

Layers within a vdW heterostructure can be twisted relative to one another, providing an additional degree of freedom for the exploration of novel quantum phenomena. Introducing a twist angle between two atomic lattices creates a new combined structure with unique properties. At certain commensurate angles, this combined structure displays a periodic **Moiré Pattern** which has a larger conventional unit cell¹ containing multiple primitive cells of the original lattices 2.1.

While 2D materials and vdW heterostructures are an exciting platform for discovering emergent condensed matter phenomena, the expanding library of 2D materials and

¹This larger unit cell is often called a “supercell”.

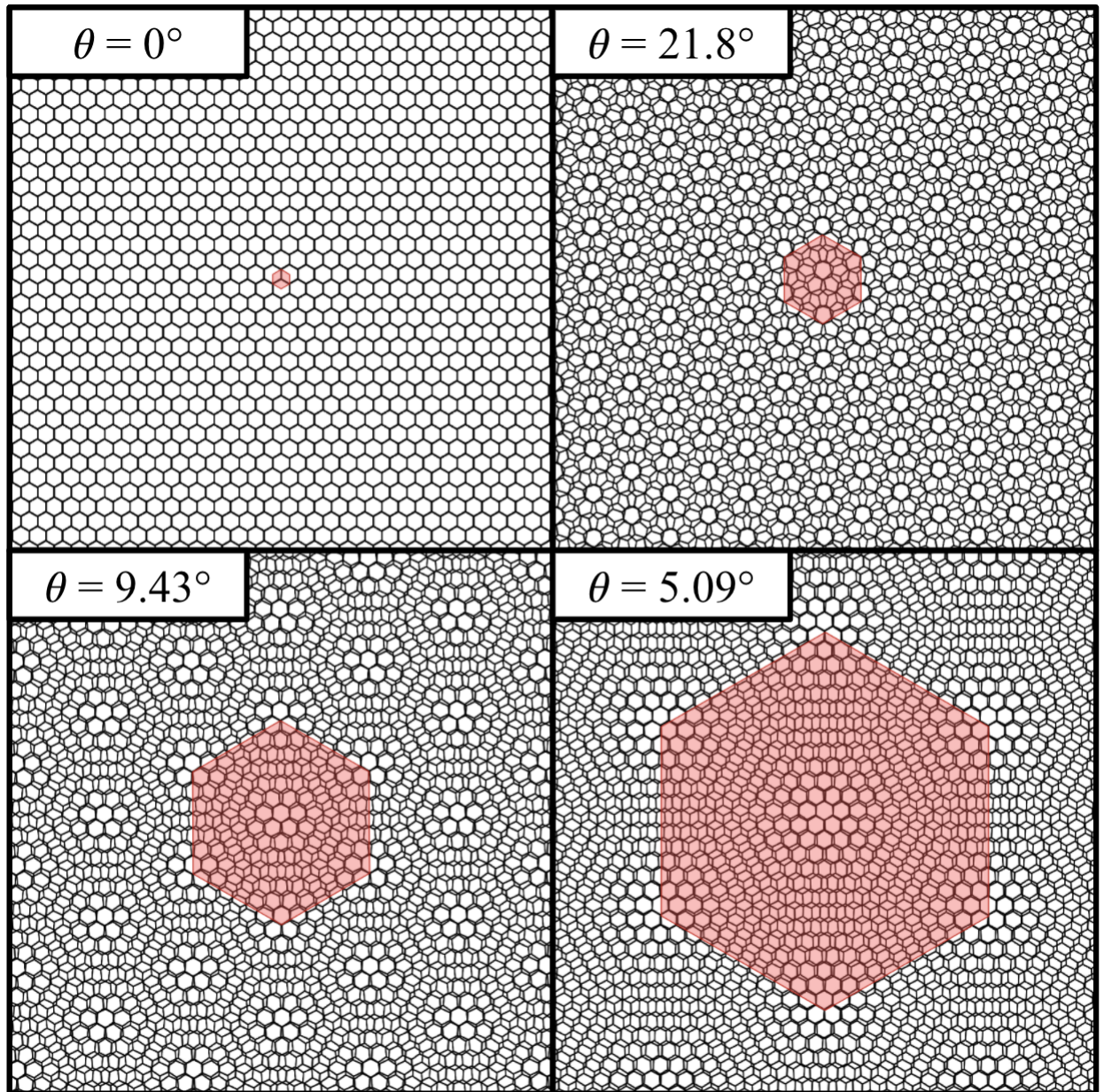


Figure 2.1: Two honeycomb lattices twisted relative to each another form periodic Moiré patterns at certain commensurate angles. The conventional unit cell of the overall Moiré pattern (red) increases in size as the twist angle (θ) decreases. When $\theta = 0^\circ$, the system is bilayer graphene and its unit cell is the same size as graphene's. When $\theta = 21.8^\circ$, the twisted bilayer supercell contains 7 graphene unit cells; when $\theta = 9.43^\circ$, the supercell contains 37 graphene unit cells; when $\theta = 5.09^\circ$, the supercell contains 127 graphene unit cells.

increasing number of vdW heterostructure possibilities makes fully exploring their capabilities an arduous task. Aside from the daunting breadth of systems, experimental work with vdW heterostructures can be difficult and expensive. Certain systems are very difficult to examine even theoretically; twisted bilayer graphene, for example, displays interesting effects at very low twist angles [7, 8] that produce very large unit cells difficult to model computationally. Prototyping and perfecting devices utilizing vdW heterostructures is a time-consuming and expensive process.

2.2 Metamaterials

Metamaterials are engineered to exhibit unique properties due to their macroscopic structure rather than their individual components. They are typically created from many elements assembled into a periodic pattern, allowing the composite structure to manipulate certain physical phenomena.

Because metamaterials' capabilities rely only on their structure, there is great flexibility in their production. So long as the basic periodic structure of a metamaterial is sustained, the size parameters and materials used to build it can be tuned to adjust the resulting physical effects as needed. We can build metamaterials at the nanoscale out of photonic crystals or at the macroscale using a 3D printer, and so on.

Metamaterials are further attractive to work with because they can mimic quantum materials. Although metamaterials have length and energy scales vastly different from quantum materials, they can be macroscopically constructed to exhibit physical phenomena similar to those of nanoscale quantum materials. Already metamaterials have been used to mimic topological insulators, quantum Hall systems, and Weyl semimetals [9, 10, 11].

2.3 Phononic Metamaterials as Quantum Mimics

Phononic metamaterials are engineered to control acoustic waves to produce interesting effects. We can therefore engineer a phononic metamaterial to manipulate the flow of ultrasound so that it mimics the way electrons move through solids, effectively creating a phonic metamaterial quantum mimic.

Electron behavior in solids is governed by the Schrödinger wave equation:

$$i\hbar \frac{\partial \psi}{\partial t} = -\frac{\hbar^2}{2m} \nabla^2 \psi,$$

which atomic orbital eigenstates that can be mapped onto the atomic lattice to produce an energy band structure.

The acoustic wave equation in a periodic solid is:

$$B_r(\vec{r}) \left(\nabla \cdot \left[\frac{1}{\rho_r(\vec{r})} \nabla p \right] \right) = -\frac{\omega^2}{c_1^2} p,$$

where p is the pressure, $\rho_r(\vec{r}) = \rho(\vec{r})/\rho_1$ is the relative mass density of the material, $B_r(\vec{r}) = B(\vec{r})/B_1$ is the relative bulk modulus of the material, and $c_1 = \sqrt{B_1/\rho_1}$ is the speed of sound in the material. The acoustic wave equation has pressure mode solutions that can be mapped onto the metamaterial lattice to produce a frequency band structure.

Although the former is quantum mechanical the latter classical, they can be solved through analogous means [12], implying not only that the atomic orbitals of the quantum material are comparable to the pressure modes of the metamaterial, but also that the band structures of the two materials should display matching features².

Viewed through a tight-binding lens, the parameters of this quantum material - phononic metamaterial analogy are as follows: the hopping particle of interest is in the quantum material the electron and in the phononic metamaterial the normal mode of an acoustic vibration, or a phonon³. Lattice hopping sites are in the quantum material atoms and in the phononic metamaterial some sort of periodic structure capable of hosting a phonon.

Phononic metamaterials present a compelling pathway for studying emergent condensed matter phenomena because they are easier to fabricate and characterize than quantum materials. These quantum mimics can be fabricated macroscopically, and their governing equations are classical and well-understood.

Phononic crystals have been engineered to mimic graphene [14] and more recently, macroscopic phononic metamaterials have been used to mimic graphene and bilayer graphene [15], presenting phononic metamaterials as an attractive platform for modeling 2D materials and vdW heterostructures.

2.4 Work Presented

This thesis develops an intuitive model for phononic metamaterial analogs of 2D materials and vdW heterostructures following tight-binding principles. This model can be used to expand our library of 2D metamaterials and vdW metamaterials, providing a compelling platform to rapidly explore and prototype interesting condensed matter phenomena.

First, I describe my “connected-cavity” model for designing 2D metamaterials according to tight-binding principles. I then create phononic metamaterial graphene.

²This phononic scheme can further be translated to photonics through simple variable-matching [13]

³A phonon is the quantum of vibration, similar to how a photon is the quantum of light [2].

Next, I extend my model to accurately mimic stacked vdW heterostructures and create all standard configurations of phononic metamaterial bilayer graphene.

Finally, I introduce a twist angle to the bilayer system to create phononic metamaterial⁴ twisted bilayer graphene, providing a pathway for achieving a magic-angle phononic flat band.

All work was conducted theoretically using the acoustics module of the commercial finite element analysis software COMSOL Multiphysics.

⁴I will henceforth drop the “phononic” specification; unless otherwise specified, all metamaterials presented in this thesis are phononic.

Chapter 3

Design Approach and Results

3.1 The Connected Cavity Model

Recall the following requirements of the tight-binding approximation:

1. Particles are bound to lattice sites.
2. The hopping parameter t is equal between all nearest-neighbor lattice sites.
3. A particle's hopping ability depends on the coupling between neighboring sites.

A phononic metamaterial mimicking a 2D quantum material through tight-binding principles must also meet these three requirements. I have thus developed what I refer to as the “connected-cavity” metamaterial model, which fulfills the above requirements as follows:

1. Lattice sites are represented in the metamaterial as cavities in a solid that can hold standing acoustic waves; in other words, phonons are bound to these cavity lattice sites.
2. The hopping parameter t is represented by the distance between cavities. The physical distance between nearest-neighbor cavities in the metamaterial is therefore made equal (see Figure 3.2).
3. Coupling in this metamaterial refers to an acoustic wave’s ability to travel from one cavity to another. Thin channels are introduced between nearest-neighbor sites to activate coupling and effectively guide the wave along allowed hopping paths.

To prevent acoustic waves from leaking out, we simply place thin bounding membranes above and below the metamaterial¹.

¹The thickness and density of these bounding layers is variable, as are the other properties of metamaterials built using this design

There are several implications to this design. Firstly and perhaps most noticeably, it is highly intuitive. Even without any understanding of the quantum materials these metamaterials mimic or the tight-binding principles they follow, we can reasonably understand the behavior of acoustic waves within them.

This design also implies great flexibility in fabrication. A connected-cavity metamaterial can be produced macroscopically at a range of sizes. The metamaterial's scale influences the frequency at which acoustic waves display interesting effects; generally, metamaterials built at smaller length scales will produce band structures with features at higher frequencies, and vice versa. There is also flexibility in the material used to fabricate a connected-cavity metamaterial. At the most abstract level, so long as the material within the connected-cavity network has a density much smaller than the surrounding material's density, the metamaterial should recognizably manipulate acoustic waves according to tight-binding principles. Intuitively, the greater the difference in densities between the two materials, the more effective the model will be. For simplicity, we would imagine the cavities would contain air and the surrounding material would be some solid².

Finally, there is room to modify the design as needed to mimic a range of 2D materials. So long as nearest-neighbor cavity sites are equally distant to each other, we can conceivably build any type of lattice as a connected-cavity metamaterial. What's more, because site coupling is controlled by physical channels connecting cavities, additional unconnected features can be inserted into the metamaterial as needed. For example, we can insert extra cavities into the honeycomb connected-cavity metamaterial without significantly altering its band structure (Figures 3.2 and 3.4). The ability to insert these extra features will prove relevant when coupling multiple metamaterial layers using tight-binding principles³.

3.2 Designing Two-dimensional Metamaterials

To create a metamaterial analog of a 2D quantum material, we must first identify the electron hopping patterns within the quantum material in question.

²In all following calculations, metamaterials were built from steel sheets containing connected air cavities, with length scales on the order of millimeters. We could, however, imagine fabricating these metamaterials from 3D-printer high-density polyethylene (HDPE), or from laser-cut acrylic.

³This also has implications for conserving resources during metamaterial fabrication. If we were, for example, 3D-printing these metamaterials, inserting extra holes could save material and reduce printing time.

3.2.1 Graphene

In graphene, carbon atoms form a honeycomb lattice with a two-atom basis. Let the two atoms be A_1 and A_2 . If we restrict electrons to nearest neighbor hopping only, an electron can hop from an A_1 atom to a surrounding A_2 atom, but not to another A_1 atom, and vice versa. If the nearest neighbor hopping energy is t , the tight-binding Hamiltonian for graphene is:

$$\hat{\mathcal{H}} = \begin{bmatrix} 0 & t \\ t & 0 \end{bmatrix}. \quad (3.1)$$

Graphene's band structure displays an isolated Dirac crossing at the K point due to its C_6 symmetry [3].

To create connected-cavity metamaterial graphene, cavities are arranged in a honeycomb pattern with a two-site basis (2SB). A_1 and A_2 cavities are coupled with connecting channels. (Figure 3.1).

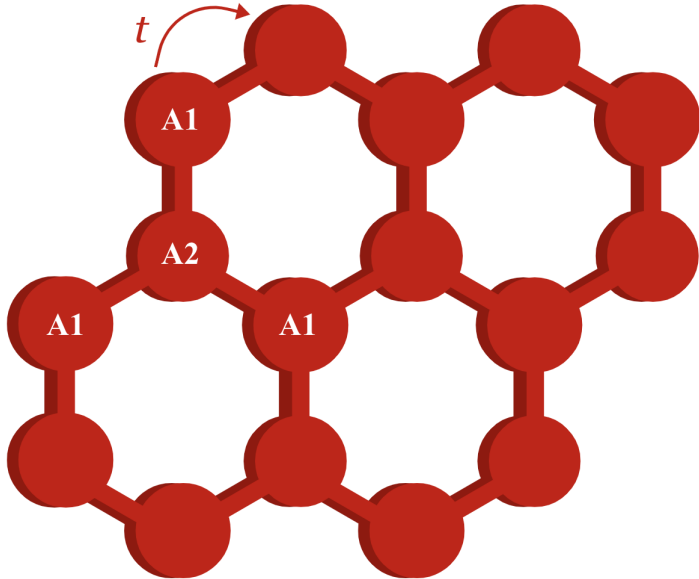


Figure 3.1: Here we visualize a 2SB honeycomb lattice of connected cavities as the basic design for phononic metamaterial graphene. Channels connect nearest neighbor hopping sites. Nearest neighbor hopping (t) occurs either from an A_1 site to an A_2 site or vice versa.

I modeled this metamaterial as air cavities in steel sandwiched between bounding HDPE layers. The metamaterial has cavity spacing (a), cavity radius (R), channel width (w), and layer thickness (D) on the order of millimeters. The band structure for this metamaterial displays an isolated Dirac-like crossing, effectively behaving like graphene for frequencies near 7.42 kHz (Figure 3.2).

I modeled this metamaterial as air cavities in steel sandwiched between bounding HDPE layers. The metamaterial has cavity spacing (a), cavity radius (R), channel width (w), and layer thickness (D) on the order of millimeters. The band structure for this metamaterial displays an isolated Dirac-like crossing, meaning the metamaterial behaves like graphene for frequencies near 7.42 kHz (Figure 3.2).

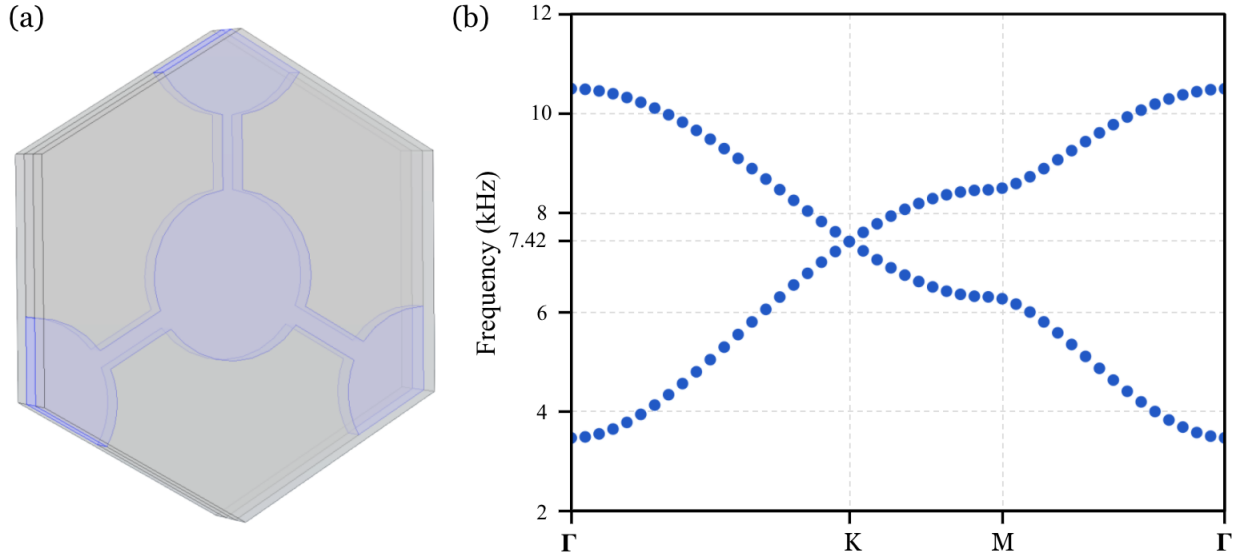


Figure 3.2: (a) This unit cell for 2SB metamaterial graphene shows air cavities in purple, steel in opaque gray, and HDPE bounding layers in semi-transparent gray. Here $a = 10$ mm, $R = 3.5$ mm, $w = R/4 = 0.875$ mm, and $D = 1$ mm. (b) The metamaterial’s resulting band structure displays an isolated Dirac-like crossing (blue) mimicking graphene.

To demonstrate the stability of this model, I introduced extra unconnected cavities throughout the metamaterial. This change is the equivalent of adding a third site (A_3) to the lattice basis. A_3 sites in this three-site basis (3SB) metamaterial graphene have zero coupling to the A_1 and A_2 sites (Figure 3.3). Let the radius of the A_3 cavities be r .

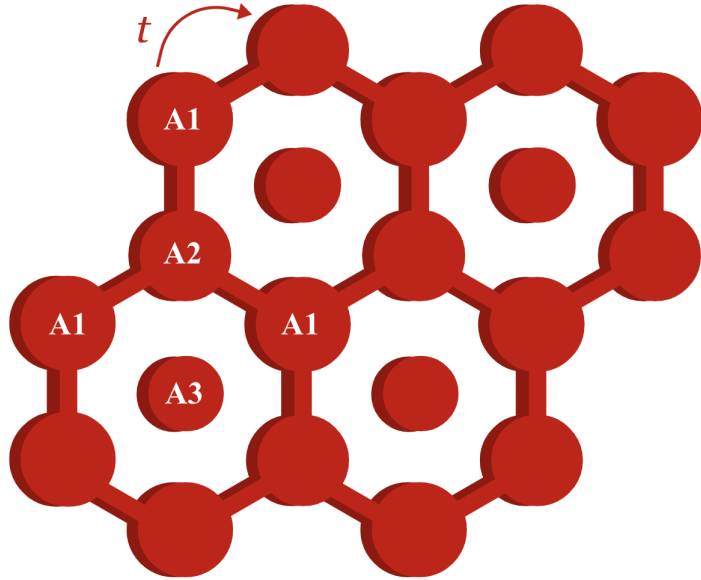


Figure 3.3: Unconnected-cavity sites (A_3) have been added to the original honeycomb lattice of connected cavities. Channels connect nearest neighbor hopping sites (with hopping energy t); there is no hopping from A_1 or A_2 sites to A_3 sites.

The tight-binding Hamiltonian for such a material is:

$$\hat{\mathcal{H}} = \begin{bmatrix} 0 & t & 0 \\ t & 0 & 0 \\ 0 & 0 & 0 \end{bmatrix}. \quad (3.2)$$

The band structure for 3SB metamaterial graphene is identical to that of 2SB metamaterial graphene, with the addition of a flat band (shown in gray) (Figure 3.4(b)). The extra band represents an isolated air mode within the extra cavities and does not affect the metamaterial’s graphene-like behavior. Altering the size of the additional cavities will change the frequency of the extra band⁴. Our ability to insert unconnected cavities without negatively impacting the metamaterial’s behavior will prove useful when extending the connected-cavity model to bilayer systems.

3.3 Designing Stacked van der Waals Metamaterials

Layered 2D materials couple together through the vdW interaction [16]. We can mimic the vdW interaction in metamaterials by placing a coupling membrane between metamaterial layers. Acoustic waves propagating in either metamaterial layer induce oscillations in the coupling membrane producing the effects of interlayer hopping; the strength Δ of this interlayer hopping can be tuned by adjusting the density and thickness of the coupling membrane [15]. To complete the stacked metamaterial, we must identify interlayer hopping patterns.

3.3.1 AB-Stacked Bilayer Graphene

Bilayer graphene is a stacked system of two honeycomb lattices, each with a two-atom basis. Let the atoms in one layer be A_1 and A_2 and the atoms in the second layer be B_1 and B_2 . We already know the hopping parameters for A_1 with A_2 and B_1 with B_2 (Equation 3.1); we must now determine how the layers interact with each other.

Bilayer graphene naturally occurs in the AB stacking configuration in which the two atomic lattices are offset so that A_2 overlaps with B_1 . There is allowed hopping Δ between the two overlapping atoms. A_1 and B_2 do not overlap, meaning no hopping is allowed between the two. The resulting Hamiltonian for AB-stacked bilayer graphene is:

$$\hat{\mathcal{H}} = \begin{bmatrix} 0 & t & 0 & 0 \\ t & 0 & \Delta & 0 \\ 0 & \Delta & 0 & t \\ 0 & 0 & t & 0 \end{bmatrix}. \quad (3.3)$$

Intralayer hopping (t) contributes one Dirac cone per graphene layer to the overall band structure. The two Dirac cones then couple through interlayer hopping to produce

⁴If the extra cavities become too large there is a risk of the air within them coupling through the solid material to the connected-cavity system, thereby altering the metamaterial’s graphene-like behavior. In this model, extra cavities with radius $r = 0.75R$ work well.

parabolic “kissing” bands at the K point [17].

To create metamaterial bilayer graphene, we might consider simply placing a coupling membrane between two connected-cavity metamaterial graphene layers. Utilizing 2SB metamaterial graphene (Figure 3.5), however, will not yield the correct band structure. Rather than achieving the expected parabolic “kissing” structure, 2SB AB-stacked metamaterial bilayer graphene’s band structure displays a triple degeneracy at the K point (Figure 3.6(b)).

This occurs because the non-overlapping sites (A_2 and B_1) were coupling partially to the steel in their respective counterpart layers. That is, oscillations in the air in A_2 and B_1 sites were propagating through the coupling membrane into solid steel, which then disturbed the acoustic waves traveling through the connected cavities enough to alter the band structure.

To remedy this issue, I built the same bilayer structure instead using 3SB metamaterial graphene (Figure 3.7).

From 3SB metamaterial graphene we learned unconnected cavities do not have intralayer coupling to the surrounding connected-cavity network. By using 3SB metamaterial graphene to make AB-stacked metamaterial bilayer graphene, A_2 and B_1 sites overlap with B_3 and A_3 sites respectively; interlayer coupling between these sites is contained and prevented from affecting the rest of the material. The tight-binding Hamiltonian for this structure is

$$\hat{\mathcal{H}} = \begin{bmatrix} 0 & t & 0 & 0 & 0 & 0 \\ t & 0 & 0 & \Delta & 0 & 0 \\ 0 & 0 & 0 & 0 & 0 & 0 \\ 0 & \Delta & 0 & 0 & t & 0 \\ 0 & 0 & 0 & t & 0 & 0 \\ 0 & 0 & 0 & 0 & 0 & 0 \end{bmatrix}. \quad (3.4)$$

The resulting band structure shows the desired parabolic “kissing” bands at the K point, mimicking AB bilayer graphene (Figure 3.8(b)).

There are two additional bands (shown in gray) representing isolated air modes within A_3 and B_3 sites, respectively. Again, altering the size of the additional cavities will change the frequencies of the extra bands⁵.

3.3.2 AA-Stacked Bilayer Graphene

AA-stacked bilayer graphene has entirely overlapping atomic layers; there is allowed hopping Δ between A_1 and B_1 sites, as well as between A_2 and B_2 sites. AA-stacked

⁵There is a balance to be reached between making the extra cavities large enough to contain interlayer coupling but small enough to avoid intralayer coupling. Again, $r = 0.75R$ works well here.

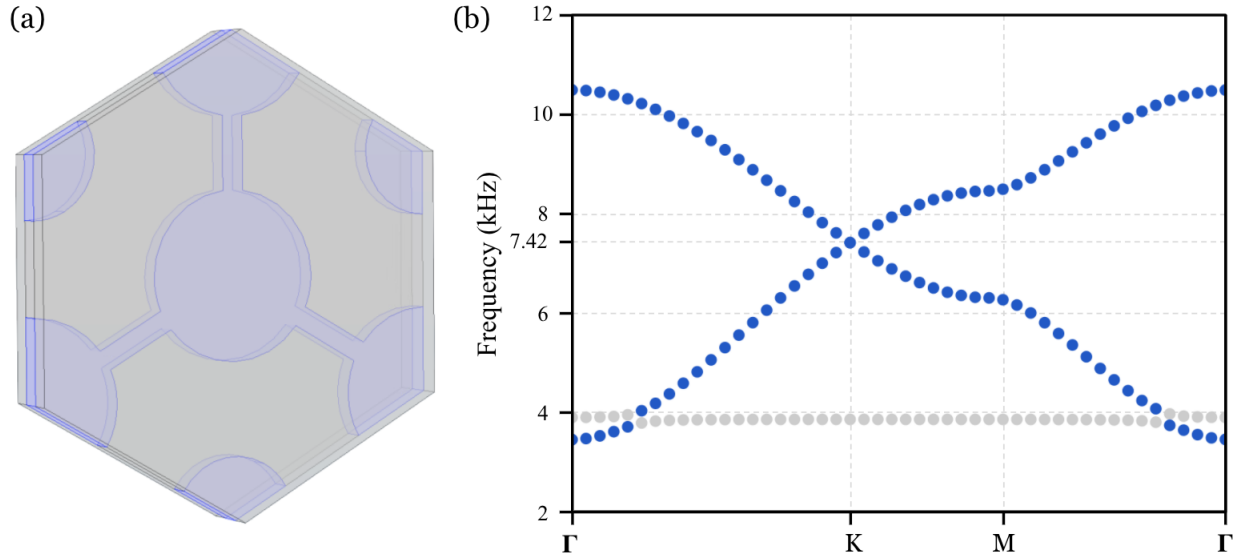


Figure 3.4: (a) The unit cell for 3SB connected-cavity metamaterial graphene has the same properties as the unit cell in Figure 3.2(a). The additional unconnected cavities have radius $r = 0.75R = 2.625$ mm. (b) The metamaterial’s resulting band structure displays an isolated Dirac-like crossing (blue) identical to the one shown in Figure 3.2(b). The extra band (gray) represents an isolated air mode within the extra cavities.

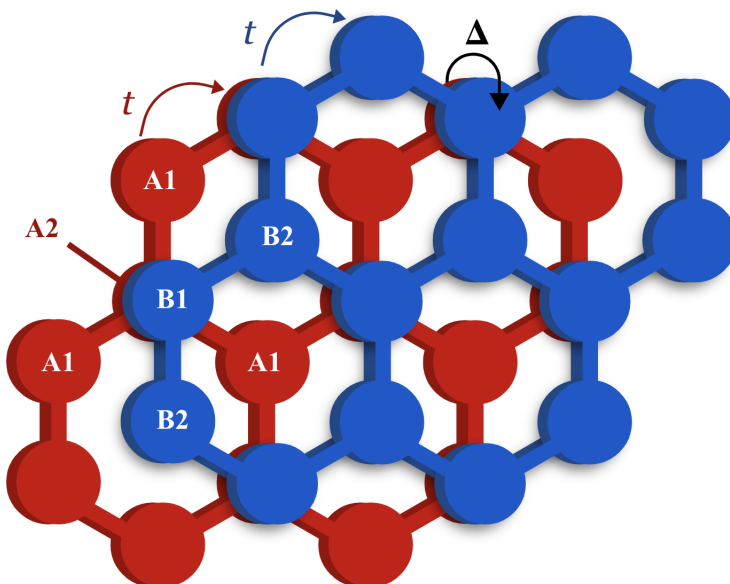


Figure 3.5: Here we visualize the coupling between 2SB honeycomb cavity networks in either layer of AB-stacked metamaterial bilayer graphene. Connective channels within each layer indicate intralayer hopping (t); Overlapping sites have interlayer hopping (Δ). A_2 and B_1 sites overlap; A_1 and B_2 do not.

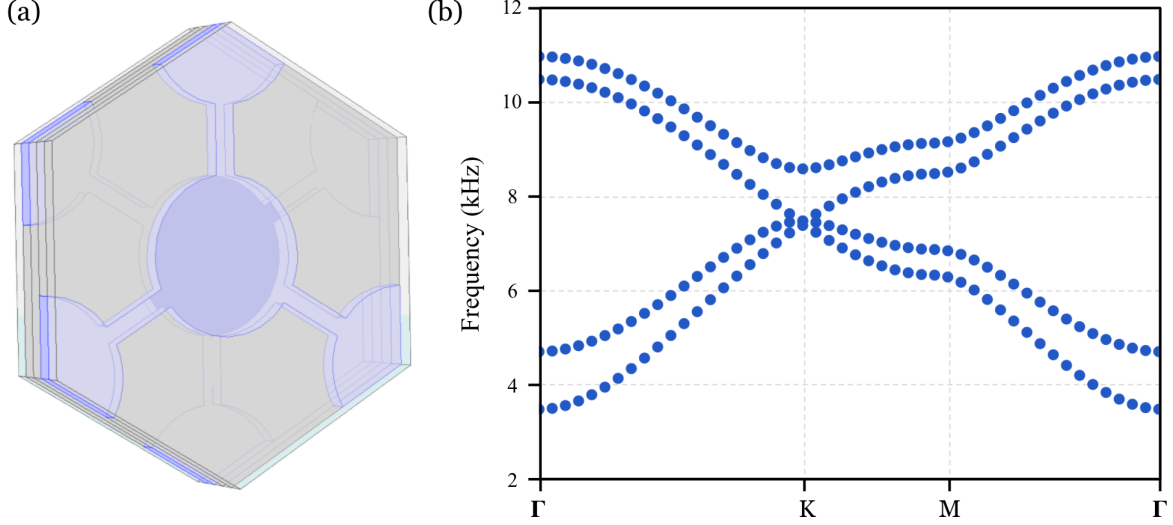


Figure 3.6: (a) This unit cell for 2SB AB-stacked metamaterial bilayer graphene shows air cavities in purple and steel in opaque gray. The metamaterial layers and outer HDPE bounding layers have the same properties (a , R , w , and D) as in Figure 3.2(a). The center coupling layer is HDPE with thickness D , identical to the outer bounding layers. (b) The metamaterial’s resulting band structure displays abnormal behavior at the K point not matching the expected parabolic “kissing” structure present in AB-stacked bilayer graphene.

bilayer graphene has the tight-binding Hamiltonian

$$\hat{\mathcal{H}} = \begin{bmatrix} 0 & t & \Delta & 0 \\ t & 0 & 0 & \Delta \\ \Delta & 0 & 0 & t \\ 0 & \Delta & t & 0 \end{bmatrix}. \quad (3.5)$$

This stacking configuration produces a band structure with two spaced Dirac crossings at the K point [16].

While AA-stacked bilayer graphene has interesting electronic properties, it is difficult to fabricate and examine, as bilayer graphene tends to relax back to the AB stacking configuration⁶ [16].

Conversely, the metamaterial’s connected-cavity sites have rigid positions and do not relax like atoms in a lattice. We can therefore easily create AA-stacked metamaterial bilayer graphene by layering two metamaterial graphene layers around a coupling membrane.

I first created 2SB AA-stacked metamaterial bilayer graphene (Figure 3.9).

⁶We mainly focus on AB and AA because they are periodic and have reasonable unit cells, but there are bilayer graphene stacking configurations beyond just AB and AA. Two layers of graphene can conceivably be stacked in any configuration. All configurations aside from AB are difficult to fabricate due to bilayer graphene’s tendency to relax back to AB stacking.

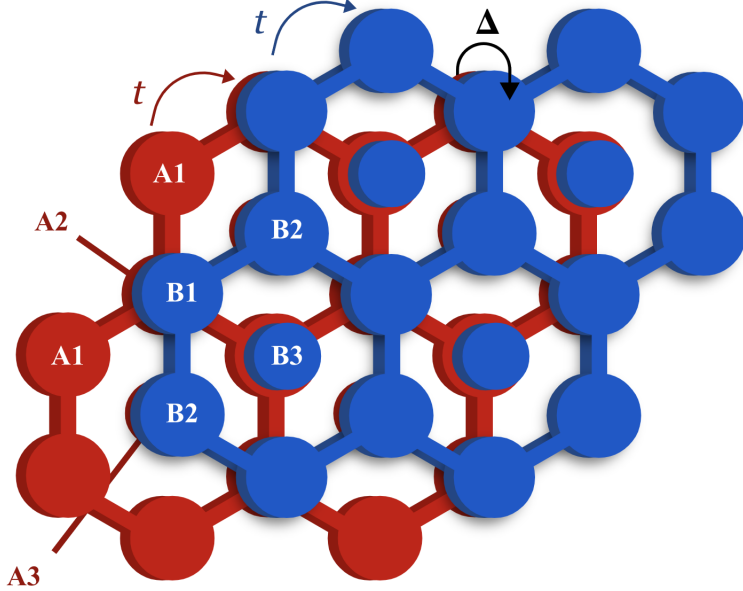


Figure 3.7: Here we visualize the coupling between 3SB honeycomb cavity networks in either layer of AB-stacked metamaterial bilayer graphene. Connective channels within each layer indicate intralayer hopping (t); Overlapping sites have interlayer hopping (Δ). A_2 and B_1 sites overlap as usual. A_1 sites overlap with B_3 sites and B_2 with A_3 .

This structure produced the desired double-Dirac-like crossing at the K point, mimicking AA-stacked bilayer graphene (Figure 3.10(b)).

For completeness, I also created 3SB AA-stacked metamaterial bilayer graphene (Figure 3.11), which has the tight-binding Hamiltonian

$$\hat{\mathcal{H}} = \begin{bmatrix} 0 & t & 0 & \Delta & 0 & 0 \\ t & 0 & 0 & 0 & \Delta & 0 \\ 0 & 0 & 0 & 0 & 0 & 0 \\ \Delta & 0 & 0 & 0 & t & 0 \\ 0 & \Delta & 0 & t & 0 & 0 \\ 0 & 0 & 0 & 0 & 0 & 0 \end{bmatrix}. \quad (3.6)$$

This structure also produced the desired double-Dirac-like crossing at the K point (Figure 3.12(b)). The two extra bands (shown in gray) again represent isolated air modes within A_3 and B_3 sites, respectively, and do not affect the graphene-like properties of the metamaterial.

This second model worked because the extra unconnected cavities (A_3 and B_3) had interlayer coupling to each other but no intralayer coupling to their respective layer's connected-cavity network. Our ability to create an accurate mimic of AA-stacked bilayer graphene with extra cavities will prove useful as we move towards mimicking twisted bilayer graphene.

3.4 Designing Twisted van der Waals Metamaterials

Introducing a twist angle between stacked 2D materials gives rise to novel and sometimes exotic physical phenomena [6, 5]. If we can extend the vdW metamaterials model to also

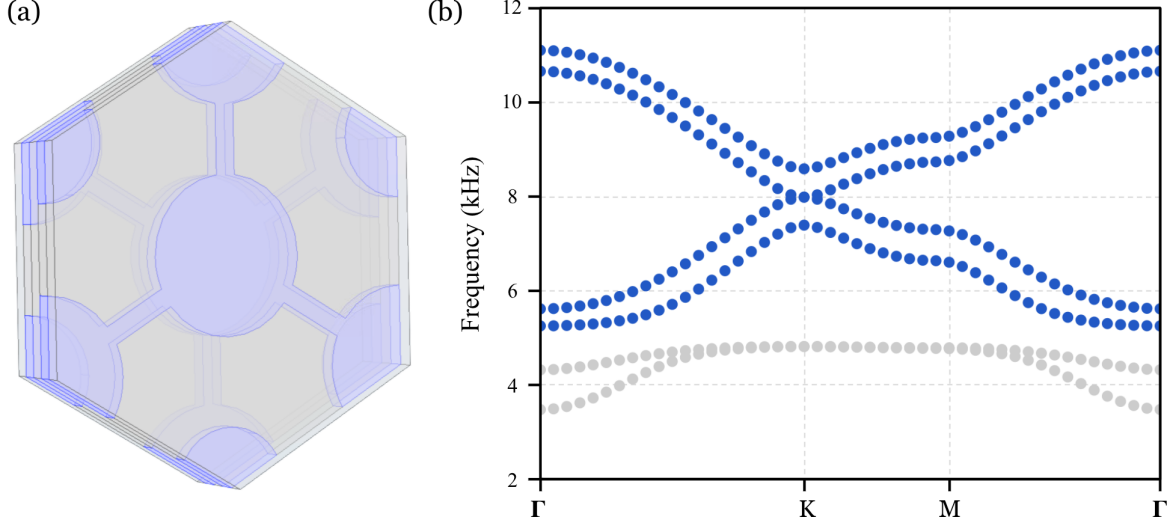


Figure 3.8: (a) This unit cell for 3SB AB-stacked metamaterial bilayer graphene has the same properties as in Figure 3.6(a), with additional unconnected air cavities ($r = 2.626$ mm). (b) The metamaterial’s resulting band structure displays parabolic “kissing” at the K point mimicking AB-stacked bilayer graphene. The extra two bands (gray) represent isolated air modes in A_3 and B_3 sites, respectively.

mimic twisted vdW heterostructures, we can confidently present the model as a means for rapidly exploring phenomena in their quantum counterparts.

For eased computation, we often consider twisted systems at commensurate twist angles that create periodic Moiré patters in the heterostructure (Figure 2.1).

3.4.1 Twisted Bilayer Graphene

Twisted bilayer graphene (TBG) has interesting band structure features, especially at lower twist angles. As the twist angle decreases, the two Dirac crossings of bilayer graphene become flatter [18, 19, 20]. Flattening bands correspond to electrons moving at slower and slower speeds. This is significant because slowed electrons are more likely to interact within a material, resulting in unconventional and exotic behavior like high-temperature superconductivity [7, 8].

Let us consider the geometry of bilayer graphene as a twist angle (θ) is introduced between layers. AB and AA are the two bilayer graphene stacking configurations that produce a periodic heterostructure. While we might consider both AA and AB-stacked bilayer graphene as untwisted models, each configuration is actually a twisted version of the other; twisting one layer in AB-stacked bilayer graphene by 60° produces AA-stacked bilayer graphene, and vice versa. Beginning twist calculations from the AB or AA stacking configuration will produce parabolic touching or linear crossing behavior at the K point, respectively. Aside from K point behavior, TBG band structures remain

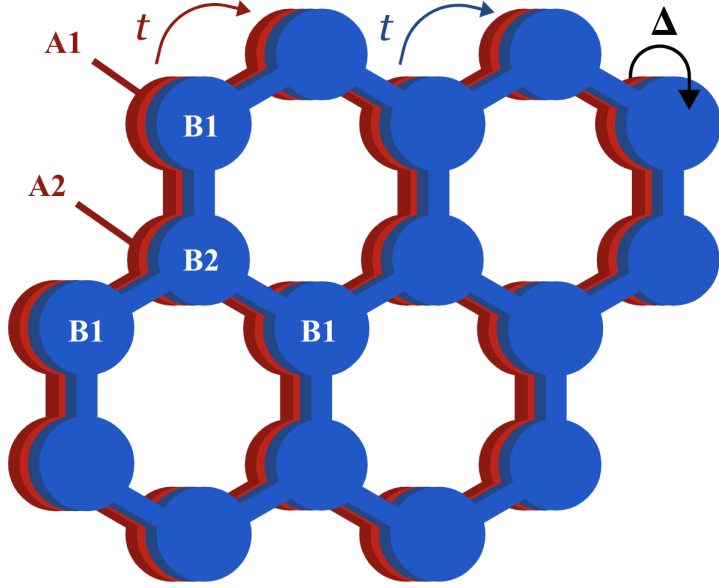


Figure 3.9: Here we visualize the coupling between 2SB honeycomb cavity networks in either layer of AA-stacked metamaterial bilayer graphene. Connective channels within each layer indicate intralayer hopping (t); Overlapping sites have interlayer hopping (Δ). Each cavity network overlaps entirely with the other; that is, A_1 sites overlap with B_1 sites and A_2 with B_2 .

largely the same between AB and AA starting configurations [20].

However, the choice of metamaterial bilayer graphene to twist is not arbitrary. As θ decreases, the TBG supercell size increases, and zones of AB and AA stacking configurations form within the overall structure (Figure 3.13). I was previously able to mimic AA-stacked bilayer graphene with both the 2SB and 3SB metamaterial graphene, but I could only mimic AB-stacked bilayer graphene with 3SB metamaterial graphene. I therefore began twisting from 3SB AA-stacked metamaterial bilayer graphene (Figures 3.11 and 3.12) to ensure AB-stacked regions in the heterostructure would be accurate.

I built 3SB metamaterial TBG unit cells for commensurate angles 21.8° , 9.43° , 6.01° , and 5.09° (Figure 3.15(a)). Their resulting band structures displayed flattening Dirac-like crossings very closely resembling features found in TBG band structures (Figure 3.15(b)⁷). From $\theta = 21.8^\circ$ to $\theta = 5.09^\circ$, the Dirac-like crossings' bandwidth decreased from 2.13 kHz to 0.06 kHz (Figure 3.14).

The incredible success of this metamaterial TBG model has several implications.

First, the metamaterial bilayer graphene design required no additional changes to be extended to metamaterial TBG. Specifically, the additional unconnected sites in the 3SB metamaterial graphene did not cause unusual behavior once the bilayer system was twisted, meaning regions of the twisted supercell that had neither AA nor AB stacking configurations were not impacted by the presence of extra cavities. Any interlayer coupling to these unconnected cavities was effectively contained and did not cause unwanted intralayer coupling.

⁷Note: the metamaterial TBG band structures span the Brillouin zone differently than previous band structures shown. Here we span the Brillouin zone from K point to K point to more easily visualize how the Dirac-like crossings flatten at different twist angles.

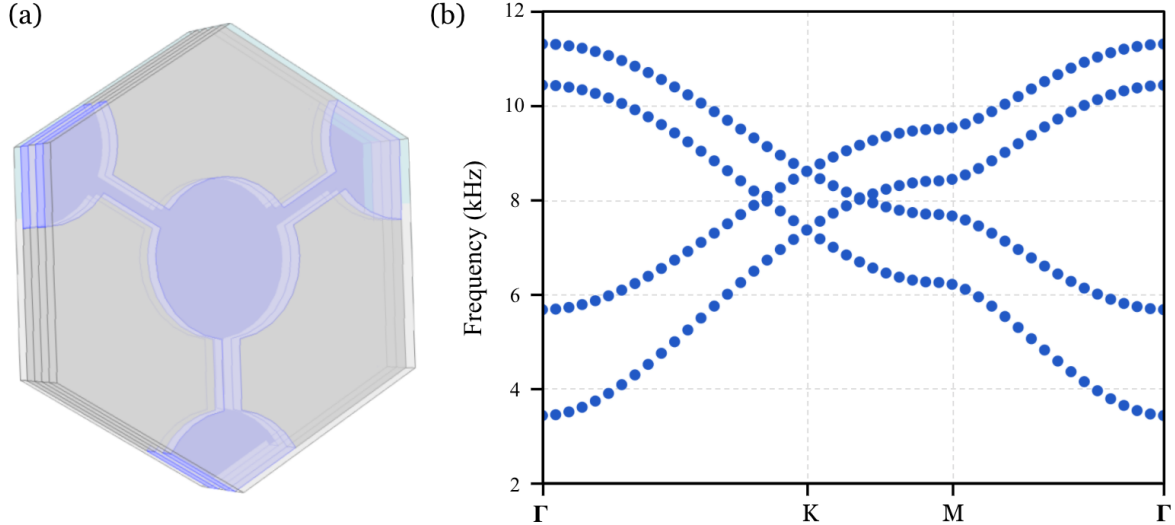


Figure 3.10: (a) This unit cell for 2SB AA-stacked metamaterial bilayer graphene has the same properties as in Figure 3.6(a), with one metamaterial layer rotated 60° so that both cavity networks entirely overlap. (b) The meta-material's resulting band structure displays double-Dirac-like crossings at the K point mimicking AA-stacked bilayer graphene.

Second, this metamaterial TBG closely mimics its quantum counterpart without relaxation effects. As mentioned previously, while atoms in bilayer graphene tend to relax back to an AB stacking configuration, sites in these phononic metamaterials are rigid; this fact allowed us to create AA-stacked metamaterial bilayer graphene just as easily as AB-stacked metamaterial bilayer graphene. However, atoms in TBG also tend to relax back to the AB stacking configuration [21]. In reference to Figure 3.13, relaxation effects in TBG would minimize the circular AA stacking regions and maximize the triangular AB stacking regions. Metamaterial TBG clearly lacks relaxation effects, yet mimics the quantum system very well.

Most important to note is that while metamaterial TBG's band structures display flattening features closely resembling those present in TBG's band structures, these features appear at much higher twist angles in the metamaterial system than in the quantum system. The twist angle at which flattening features appear is dependent on interlayer coupling in system; in general, the greater the coupling between the two graphene layers, the higher the twist angle at which we see flatter features. In TBG, coupling is increased by applying pressure to the system, which can be difficult to achieve experimentally [22]. In metamaterial TBG, however, interlayer coupling is controlled by the density and thickness of the coupling membrane [15]. The coupling membrane's properties can be tweaked easily to pull interesting flat features up to higher twist angles. Higher twist angles result in smaller TBG supercells (see Figures 2.1 and 3.14(a)), which are far easier to

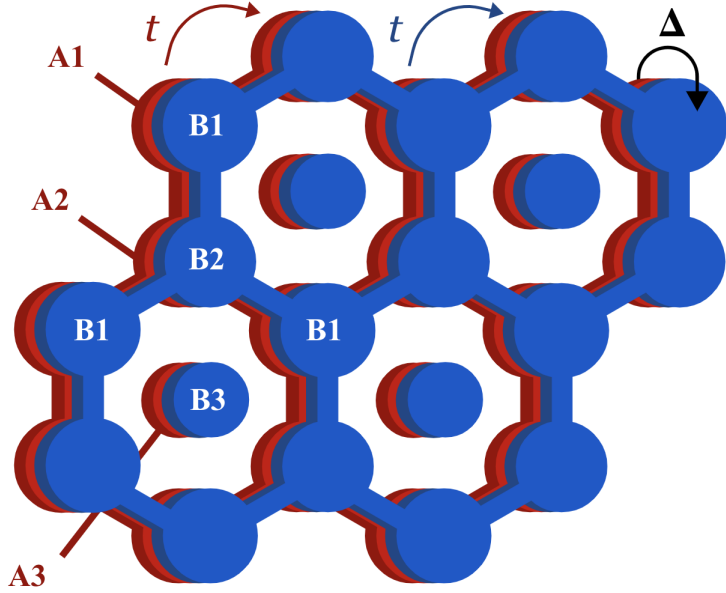


Figure 3.11: Here we visualize the coupling between the 3SB honeycomb cavity networks in either layer of AA-stacked metamaterial bilayer graphene. Connective channels within each layer indicate intralayer hopping (t); Overlapping sites have interlayer hopping (Δ). There is overlap between A_1 and B_1 , A_2 and B_2 , and A_3 and B_3 sites.

computationally model than the larger supercells created from very small twist angles⁸.

⁸In fact, the metamaterial TBG band structures presented in this paper each took a few hours (or less) to generate. Compared to the *days* required to run band structure calculations for quantum systems, a few hours is a massive improvement.

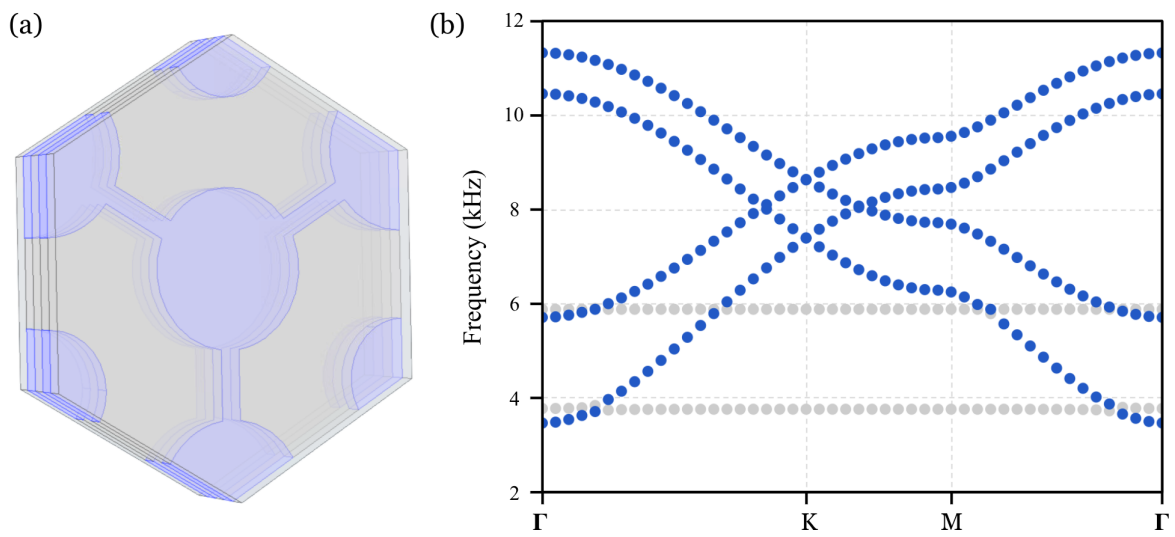


Figure 3.12: (a) This unit cell for 3SB AA-stacked metamaterial bilayer graphene has the same properties as in Figure 3.8(a), with one metamaterial layer rotated 60° so that both cavity networks entirely overlap. (b) The metamaterial's resulting band structure retains the expected double-Dirac-like crossings at the K point seen in Figure 3.10(b). The extra two bands (gray) represent isolated air modes in A_3 and B_3 sites, respectively.

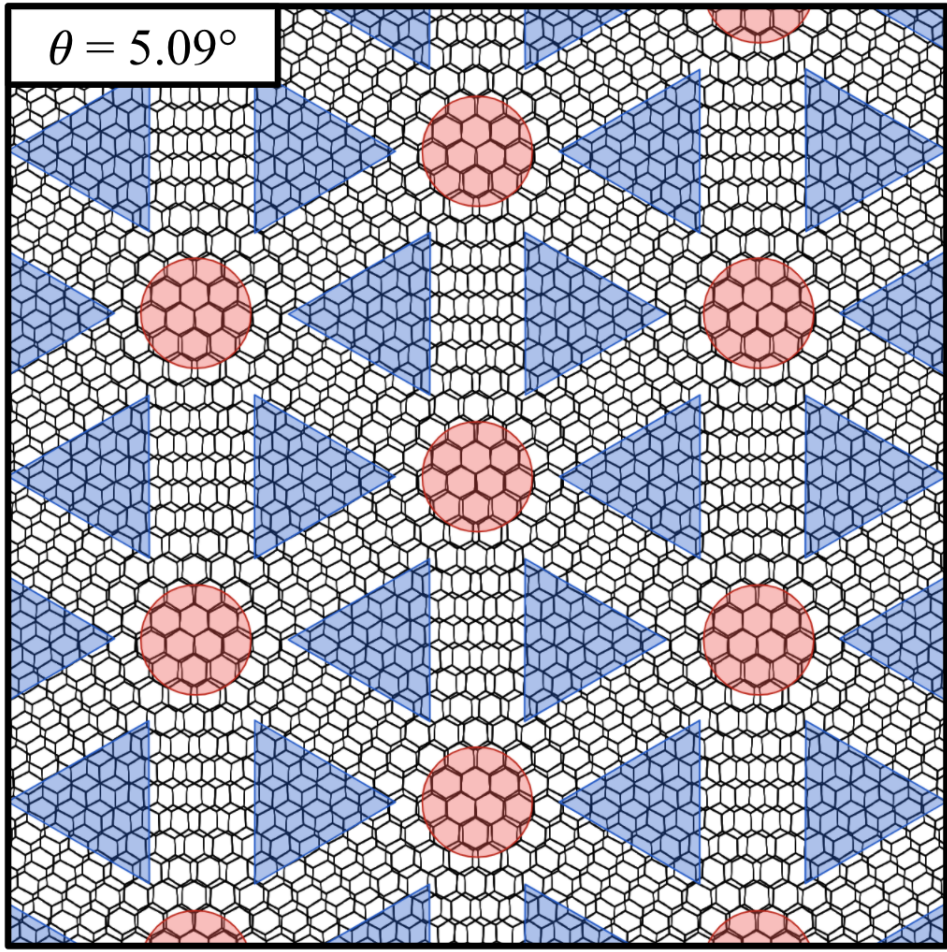


Figure 3.13: TBG has regions of AB stacking (blue triangles) and AA stacking (red circles) connected by transition regions that have neither AA nor AB stacking.

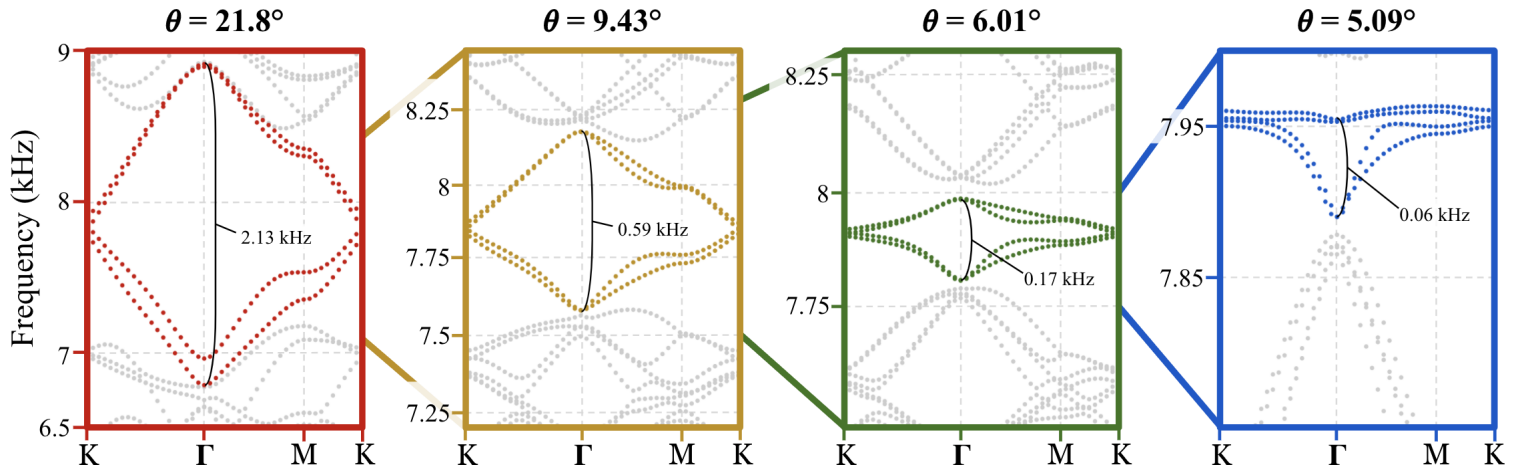


Figure 3.14: The Dirac-like crossings (blue) originally present in 3SB AA-stacked metamaterial bilayer graphene become flatter as θ decreases. Each band structure spans a smaller frequency range than the previous. Extra bands (gray) represent various other modes in the TBG heterostructure and are not relevant to the flattening bands.

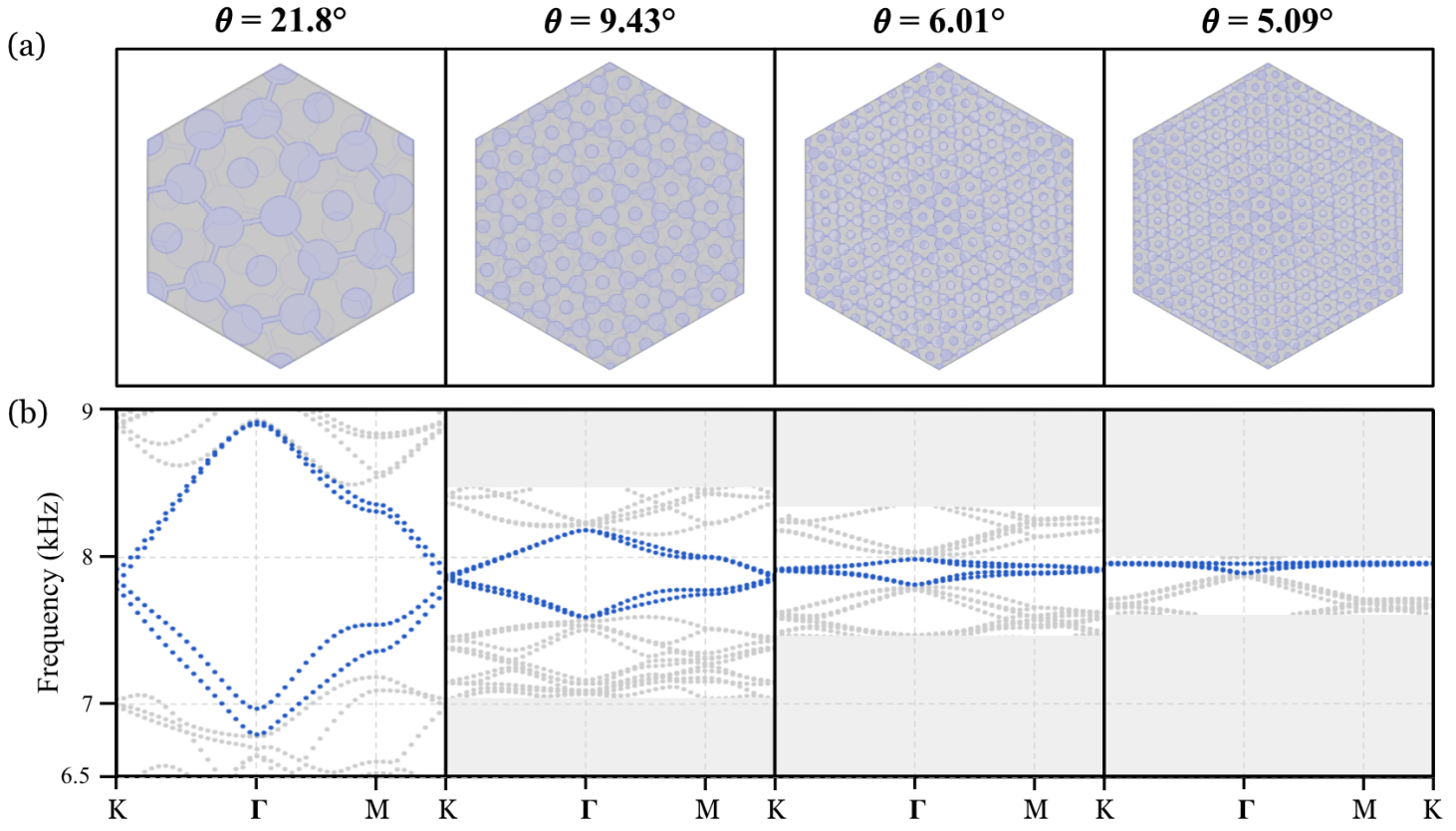


Figure 3.15: (a) The metamaterial TBG supercells grow in size as θ decreases. Each supercell is composed of two 3SB metamaterial graphene layers (Figure 3.4) with an intervening HDPE coupling membrane, all sandwiched between two outer HDPE bounding membranes. As in all previously shown models, $a = 10$ mm, $R = 3.5$ mm, $r = 2.625$ mm, $w = 0.875$ mm, and $D = 1$ mm. (b) The band structures from Figure 3.14 are shown here plotted on the same frequency scale to visualize the flattening effect. Data is unavailable for the gray regions in the latter three band structures, but would contain additional extra bands (gray) irrelevant to the flattening Dirac-like crossings (blue).

Chapter 4

Conclusion and Future Works

4.1 Expanding the Library of Two-dimensional Metamaterials

Obviously, to use vdW metamaterials to rapidly prototype and screen their quantum counterparts, the library of 2D metamaterials must be expanded. Using the connected-cavity model presented here, we can carry out that expansion by developing new 2D metamaterials, which can then be stacked and twisted to create new vdW metamaterials.

The first additional 2D metamaterial we may consider designing is metamaterial hexagonal boron nitride (hBN). It shares the overall honeycomb geometry of graphene, but is actually composed of two triangular lattices of boron and nitrogen, respectively. We might also consider it a 2SB honeycomb lattice where A_1 atoms are boron and A_2 atoms are nitrogen. Because hBN does not have perfect C_6 symmetry, the Dirac crossing is gapped out at the K point [23].

We might consider creating metameterial hBN by using the same connected-cavity lattice as metamaterial graphene but with altered cavity radii corresponding to boron-like and nitrogen-like sites.

4.2 Magic-Angle Metamaterial Twisted Bilayer Graphene

TBG has been shown to superconduct at certain “magic” angles that flatten the Dirac crossings completely [19, 20, 7, 8]. As a result, TBG has further promoted vdW heterostructures as a compelling platform for studying poorly understood correlated behavior.

Already my results for metamaterial TBG reflect the ability to adjust the twist angle at which we see flatter features. Although COMSOL metamaterial TBG simulations are

restricted to commensurate angles, we can tweak the coupling membrane to achieve a flat band at a commensurate angle, effectively turning it into a magic angle. We can further alter the coupling membrane to achieve flat bands at relatively high commensurate angles for greater computational ease.

Creating metamaterial magic-angle TBG would not only give us a platform to study its quantum counterpart, but also yield interesting and useful phononics. A phononic flat band is equivalent to a localized vibrational wave or “frozen” sound. Metamaterials with phononic flat bands can be interesting platforms for non-linear acoustics and may aid the field of super-resolution imaging.

4.3 Flat Band Metamaterials

While this thesis explored the potential to translate interesting quantum physics to the phononic realm for the purposes of exploration, we can also use metamaterials to translate interesting phononics to the quantum realm. By taking advantage of the tight-binding-like connected-cavity model, we can design 2D metamaterials that produced flat bands simply based on their cavity lattice geometry.

For example, the kagome lattice displays a flat band in its band structure due to destructive interference in electron hopping that confines electrons to certain sites [24]. We can create a connected-cavity metamaterial build with a kagome lattice of cavities to create a phononic flat band. We can further explore how tweaking the lattice geometry can further flatten this band, resulting in better phonon localization. Such an exploration could provide the blueprints for an eventual flat band quantum material.

References

- [1] Neil W. Ashcroft and David N. Mermin. *Solid State Physics*. Holt, Rinehart and Winston, 1976.
- [2] Steven H. Simon. *The Oxford Solid State Basics*. Oxford University Press, 2013.
- [3] Andrey K. Geim and Allan H. Macdonald. “Graphene: Exploring carbon flatland”. In: *Physics Today* 60.8 (2007), pp. 35–41. DOI: [10.1063/1.2774096](https://doi.org/10.1063/1.2774096).
- [4] A. K. Geim and I. V. Grigorieva. “Van der Waals heterostructures”. In: *Nature* 499.7459 (2013), p. 419. DOI: [10.1038/nature12385](https://doi.org/10.1038/nature12385).
- [5] K. S. Novoselov et al. “2D materials and van der Waals heterostructures”. In: *Science* 353.6289 (2016), aac9439. DOI: [10.1126/science.aac9439](https://doi.org/10.1126/science.aac9439).
- [6] Pulickel Ajayan, Philip Kim, and Kaustav Banerjee. “Two-dimensional van der Waals materials”. In: *Physics Today* 69.9 (2016), pp. 38–44. DOI: [10.1063/PT.3.3297](https://doi.org/10.1063/PT.3.3297).
- [7] Yuan Cao et al. “Correlated insulator behaviour at half-filling in magic-angle graphene superlattices”. In: *Nature* 556.7699 (2018), pp. 80–84. DOI: [10.1038/nature26154](https://doi.org/10.1038/nature26154).
- [8] Yuan Cao et al. “Unconventional superconductivity in magic-angle graphene superlattices”. In: *Nature* 556.7699 (2018), pp. 43–50. DOI: [10.1038/nature26160](https://doi.org/10.1038/nature26160).
- [9] Lisa M. Nash et al. “Topological mechanics of gyroscopic metamaterials”. In: *Proceedings of the National Academy of Sciences* 112.47 (2015), p. 14495. DOI: [10.1073/pnas.1507413112](https://doi.org/10.1073/pnas.1507413112).
- [10] Zheng Wang et al. “Observation of unidirectional backscattering-immune topological electromagnetic states”. In: *Nature* 461.7265 (2009), p. 772. DOI: [10.1038/nature08293](https://doi.org/10.1038/nature08293).
- [11] Ling Lu et al. “Experimental observation of Weyl points”. In: *Science* 349.6248 (2015), p. 622. DOI: [10.1126/science.aaa9273](https://doi.org/10.1126/science.aaa9273).
- [12] Jiuyang Lu et al. “Dirac cones in two-dimensional artificial crystals for classical waves”. In: *Physical Review B* 89.13 (2014), p. 134302. DOI: [10.1103/PhysRevB.89.134302](https://doi.org/10.1103/PhysRevB.89.134302).

- [13] Jun Mei et al. “First-principles study of Dirac and Dirac-like cones in phononic and photonic crystals”. In: *Physical Review B* 86.3 (2012), p. 035141. DOI: [10.1103/PhysRevB.86.035141](https://doi.org/10.1103/PhysRevB.86.035141).
- [14] Ze-Guo Chen et al. “Accidental degeneracy of double Dirac cones in a phononic crystal”. In: *Scientific Reports* 4.4613 (2014). DOI: doi.org/10.1038/srep04613.
- [15] William Dorrell et al. “van der Waals Metamaterials”. In: *Physical Review B* 101.12 (2020), p. 121103. DOI: [10.1103/PhysRevB.101.121103](https://doi.org/10.1103/PhysRevB.101.121103).
- [16] P. L. de Andres, R. Ramírez, and J. A. Vergés. “Strong covalent bonding between two graphene layers”. In: *Physical Review B* 77.4 (2008), p. 045403. DOI: [10.1103/PhysRevB.77.045403](https://doi.org/10.1103/PhysRevB.77.045403).
- [17] Edward McCann and Mikito Koshino. “The electronic properties of bilayer graphene”. In: *Reports on Progress in Physics* 76.5 (2013), p. 056503. DOI: [10.1088/0034-4885/76/5/056503](https://doi.org/10.1088/0034-4885/76/5/056503).
- [18] S. Shallcross et al. “Electronic structure of turbostratic graphene”. In: *Physical Review B* 81.16 (2010), p. 165105. DOI: [10.1103/PhysRevB.81.165105](https://doi.org/10.1103/PhysRevB.81.165105).
- [19] E. Suárez Morell et al. “Flat bands in slightly twisted bilayer graphene: Tight-binding calculations”. In: *Physical Review B* 82.12 (2010), 121407(R). DOI: [10.1103/PhysRevB.82.121407](https://doi.org/10.1103/PhysRevB.82.121407).
- [20] Pilkyung Moon and Mikito Kosino. “Optical Absorption in Twisted Bilayer Graphene”. In: *Physical Review B* 87.20 (2013), p. 205404. DOI: [10.1103/PhysRevB.87.205404](https://doi.org/10.1103/PhysRevB.87.205404).
- [21] Nguyen N. T. Nam and Mikito Koshino. “Lattice relaxation and energy band modulation in twisted bilayer graphene”. In: *Physical Review B* 96.7 (2017), p. 075311. DOI: [10.1103/PhysRevB.96.075311](https://doi.org/10.1103/PhysRevB.96.075311).
- [22] Stephen Carr et al. “Pressure dependence of the magic twist angle in graphene superlattices”. In: *Physical Review B* 98.8 (2018), p. 085144. DOI: [0.1103/PhysRevB.98.085144](https://doi.org/10.1103/PhysRevB.98.085144).
- [23] Gwan-Hyoung Lee et al. “Electron tunneling through atomically flat and ultrathin hexagonal boron nitride”. In: *Applied Physical Letters* 99.24 (2011), p. 243114. DOI: [10.1063/1.3662043](https://doi.org/10.1063/1.3662043).
- [24] Rodrigo A. Vicencio and Magnus Johansson. “Discrete flat-band solitons in the kagome lattice”. In: *Physical Review A* 87.6 (2013), 061803(R). DOI: [10.1103/PhysRevA.87.061803](https://doi.org/10.1103/PhysRevA.87.061803).